Eur. Phys. J. B **45**, 129–136 (2005)
DOI: 10.1140/epjb/e2005-00171-x

The European Physical Journal B

Time-dependent transport properties in quantum well with thin inserted layer

Zhenhong Dai[1,2,a] and Jun Ni[1]

[1] Department of Physics, and Key Laboratory of Atomic and Molecular Nanoscience, Tsinghua University, 100084, P.R. China
[2] Department of Physics, Yantai University, 264005, P.R. China

Received 12 October 2004 / Received in final form 17 January 2005
Published online 16 June 2005 – © EDP Sciences, Società Italiana di Fisica, Springer-Verlag 2005

Abstract. We investigate the time-dependent transport properties of quantum well on the situation of nonlinear bias, where a thin potential well layer is inserted in the main quantum well. In our calculations, we consider the effects from all kinds of phonon interactions in the device. We find that the charge redistribution and electron motion in the whole structure play an important effect on the final current-voltage (I-V) curve. We also find an evident current hysteresis region and current high-frequency oscillation with time in this particular region. The results show that the inserted potential well layer can make the current hysteresis width narrower than that in the single quantum well structure, and it also damps the current oscillation. Due to the existence of the inserted layer, the plateau structure of I-V curve found in the single quantum well disappears.

PACS. 73.40.Gk Elasticity, elastic constants – 73.23.Hk Coulomb blockade; single-electron tunneling – 73.50.-h Electronic transport phenomena in thin films

1 Introduction

Recently, the double-barrier resonant tunneling nanostructure has been extensively studied due to their various potential device applications and their significance in the study of confined structures. There are many important experimental researches, which include the observation of tristability [1,2], the spatial variation of the quantum-well wavefunction [3], spin-split states [4], and excitonic dark states in the quantum well [5]. Comparing with other nanostructures, double-barrier structure can be controlled very easily and can be formed on a large scale, so this particular structure is considered to be the basis for the future nanodevices. Both dc and ac transport characteristics of the system have been studied, but most of experimental researches focus on the dc transport properties, such as linear and nonlinear response, as well as time-response and carrier leakage [6–8]. In the linear transport regime, current fluctuations are generally a result of quantum interference effects and consequently are governed by the phase coherence of electrons. The physical properties of this linear regime are very clear. Now the current transport research focuses on the nonlinear transport properties. Some of these studies are based on the simulations of a realistic device using the detailed numerical procedures [9,10], while others are based on simple discrete models [11,12]. The effect of time-dependent transient current and charge density variations in the case of the nonlinear bias is very important both in ac and dc conductance. These time-dependent nonlinear characteristics may find the application in the future high-frequency device.

Early at the end of the 1980s the experimental current-voltage (I-V) characteristics of resonant transport through a double-barrier AlGaAs/GaAs/AlGaAs quantum-well shows bistability and a plateaulike structure [13]. The normal Chang-Esaki-Tsu (CET) theory [14] cannot explain the complicated experimental results. This original experimental results were explained by the current oscillations in the external circuit [15]. When the experimental conditions were improved to eliminate these oscillations, the hysteresis was removed and a smooth I-V curve with negative differential resistance region was recovered [16]. However, along with samples were made with higher or wider collector barriers specially designed to enhance charge buildup in the central QW [17–19], both bistability and hysteresis in the I-V curves appear again, which is explained theoretically by the electrostatic feedback caused by the space-charge buildup in the QW [20]. Later numerical simulations suggested that there may be intrinsic high frequency oscillations associated with coupling between the central QW and the emitter QW (formed under bias), and this coupling affects the bistability and plateaulike structures [9,10]. In recent years, the current hysteresis has also been found in the quantum wells of many other materials [21–25].

Now, some new structures have been fabricated, such as resonant tunneling diodes that incorporate a single

[a] e-mail: zhdai@ytu.edu.cn

layer of InAs quantum dots in the center of the GaAs quantum well [26,27], as well as a monolayers InAs potential well or AlAs potential barrier [28,29]. This inserted layer can affect the charge redistribution and has an important effect on the current transport in the device. There are many other studies about physical properties of this quantum well with the inserted layer, which include the quantum Hall liquid transitions [30], the magnetotunneling [31], and luminescence spectra [32]. In this paper, we study a thin potential well layer embedded in a GaAs main quantum well, and consider the effects of potential well layer on the electronic charge density redistribution and electron motion.

This paper is organized as follows: In Section 2, we briefly describe the numerical technique used in this paper. The numerical results and discussion about the time-dependent transport and electron and current distribution are presented in Section 3. The conclusion of this paper is given in Section 4.

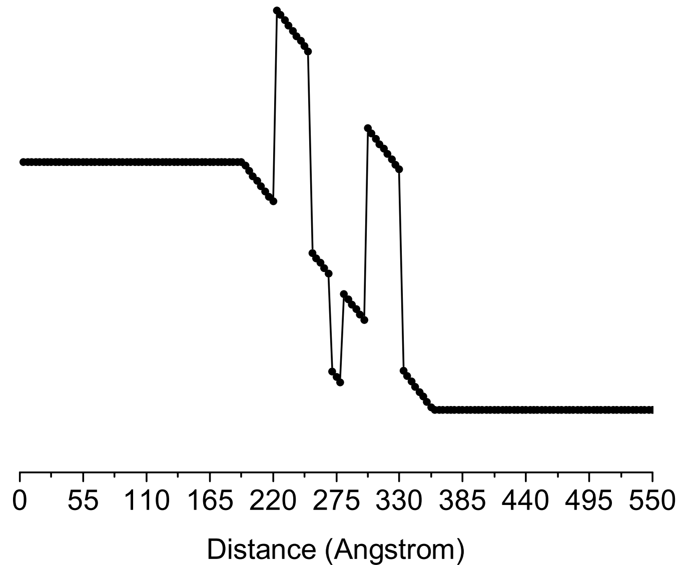

Fig. 1. The conduction-band diagram of device under certain bias.

2 Methods

The response of the system to external disturbances shows many interesting physical phenomena. For example, a longitudinal electric field, applied to a charged system, will lead to a flow of current. In many-body system of solid state physics, the conventional transport equation is Boltzmann equation, which use distribution function $f(p, R, T)$ to describe the particles motion. But Boltzmann equation is appropriate only for systems with weak, short-ranged forces and can not be applied in the nanostructures. The most significant feature of nanodevices is their small size. Due to the effect of the small size of nanodevices, some concepts concerning transport in nanodevices should be modified, such as scattering from phonons, impurities, interfaces, and electrons, dynamical screening, etc. In such devices, the wavelike nature of carriers can dominate the main characteristics of the devices, and the nanodevices exhibit very desirable device properties such as low power, high-density integration, high speed, and high-cut off frequency. Furthermore, because of the small dimension of the quantum devices, a very small bias voltage applied on the device can cause a very strong electric field in the devices. Thus, the carriers in the device are in a state far from the equilibrium state. Besides this, the transport processes become non-Markovian due to memory effects induced by scattering. Therefore, nonequilibrium and nonlinear quantum transport theories, which suitably dealt with strong fields and scatterings, are needed to describe the transport of carriers in nanodevices. In the nanodevice simulation, there are two kinds of simulation methods to be used. The first is the Monte Carlo method, which is basically a statistical method. The second is the method based upon physical transport equations, which include the density matrix method, Wigner distribution function method, the numerically solving Schrödinger equation method, and Green's function method. We use Wigner function method in our simulation of nanodevices and will introduce it in the following.

We consider an AlGaAs/GaAs/AlGaAs main quantum well with thin InAs potential well layer, and the conduction-band diagram under certain bias is shown in Figure 1. The presence of the spacer layer before the left barrier ensures that transport occurs from 2D- and 3D-electron gas coexisted in an accumulation layer at the left-hand emitter barrier [33]. The potential difference between the emitter and drain is roughly proportional to the total voltage drop V across the device. The middle potential well is the inserted layer which can modulate the electron motion in the main well. This potential is the self-consistent results from the Wigner dynamic equation and Poisson equation.

Our method is a self-consistent calculation to the Wigner-Possion equation. The Wigner function formulation of quantum mechanics has been used. It has many useful characteristics in the simulation of quantum-effect electronic devices, including ability to handle dissipated and open-boundary systems naturally. The Wigner function equation (WFE) can be derived in several ways [34]. Since the Wigner function can be defined by nonequilibrium Green's functions, the WFE can also be derived from the equation of motion of the nonequilibrium Green's function [35]. With the lowest-order approximation to the scattering, the time-dependent dynamic equation for quantum transport is

$$\frac{\partial f(x,k)}{\partial t} = -\frac{\hbar k}{m^*}\frac{\partial f(x,k)}{\partial x} - \frac{1}{\hbar}\int_{-\infty}^{\infty}\frac{dk'}{2\pi} f(x,k')\, V(x,k-k') + \left.\frac{\partial f(x,k)}{\partial t}\right|_{coll}, \quad (1)$$

where the kernel of the potential operator is given by

$$V(x,k-k') = \int_0^L dr \sin[(k-k')r][U(x+r/2) - U(x-r/2)]. \quad (2)$$

m^* is the electron effective mass, x and r is the Wigner-Weyl transformation coordinate [31], and U is the conduction-band edge. $f(x,k)$ is the Wigner function, which is defined as

$$f(x,k) = \int dr\, \rho(x+r/2, x-r/2)\exp(-ikr), \quad (3)$$

where ρ is the electron density operator. Appropriately treating scattering in semiconductors is very important for getting reasonable simulation results. Recent research shows that the computation burden associated with detailed consideration of electron-phonon scattering is formidable. The amount of computation time would be too huge if we treated the scattering in detail. Thus, we employ the relaxation-time approximation to deal with the scattering in this paper. In terms of the relaxation time approximation to scattering, the collision terms in the above equation may be written as [9]

$$\frac{\partial f(x,k)}{\partial t} = \frac{1}{\tau}\left[\frac{f_0(x,k)}{\int f_0(x,k)\,dk}\int f(x,k)\,dk - f(x,k)\right], \quad (4)$$

where τ is the relaxation time and f_0 is the equilibrium Wigner function. The boundary conditions are

$$f(0,k)|_{k>0} = \frac{m^* k_B T}{\pi\hbar^2} \times \ln\left\{1+\exp\left[-\frac{1}{k_B T}\left(\frac{\hbar^2 k^2}{2m^*} - \mu_0\right)\right]\right\}, \quad (5)$$

$$f(L,k)|_{k<0} = \frac{m^* k_B T}{\pi\hbar^2} \times \ln\left\{1+\exp\left[-\frac{1}{k_B T}\left(\frac{\hbar^2 k^2}{2m^*} - \mu_L\right)\right]\right\}. \quad (6)$$

Another important equation in our model is the Poisson equation (PE)

$$\frac{d^2}{dx^2}u(x) = \frac{q^2}{\varepsilon}[N_d(x) - n(x)], \quad (7)$$

where ε is the dielectric permittivity, $u(x)$ is the electrostatic potential, q is the electronic charge, $N_d(x)$ is the concentration of ionized dopants, and $n(x)$ is the density of electrons, which is given by

$$n(x) = \int_{-\infty}^{\infty} \frac{dk}{2\pi} f(x,k). \quad (8)$$

The corresponding current density may be written as

$$j(x) = \int_{-\infty}^{\infty} \frac{dk}{2\pi}\frac{\hbar k}{m^*} f(x,k). \quad (9)$$

To solve the WFE-PE equations, we must discretize the simulation zone and these WFE-PE equations. The details of the discretization of the WFE are well described by Frensley and Jensen et al. [9,36]. So, only a summary of the results is given here. We use the finite difference method to solve the equation (1). Assuming the simulation zone is between x=0 and x=L, the zone may be discretized as follows:

$$f(x,k) = f(x_i, k_j) = f_{ij}. \quad (10)$$

The coordinate x is discretized as

$$x_i = (i-1)L/(N_x - 1) = (i-1)\delta x \quad \delta x = L/N_x.$$

The k is discretized as

$$k_j = (2j - N - 1)\delta k/2, \; \delta k = \pi/(N\delta x).$$

N_x and N are the number of x and k points on a grid in phase space. Using the second-order upwind difference scheme to discretize the position derivative, we get

$$T\cdot f = -\frac{\hbar^2 k}{m^*}\frac{\partial f}{\partial x} = A(j)\begin{cases} f(i+2,j) - 4f(i+1,j) + 3f(i,j) & j \le N/2,\ k_j < 0 \\ -f(i-2,j) - 4f(i-1,j) - 3f(i,j) & j > N/2,\ k_j > 0 \end{cases} \quad (11)$$

where

$$A(j) = \frac{\hbar^2 \delta k}{4m^* \delta x}(2j - n - 1), \quad (12)$$

$$V\cdot f = \sum_{j'=1}^{N} V(i, j-j') f(i,j), \quad (13)$$

$$V(i,j) = \frac{2}{N}\sum_{i'=1}^{N/2} \sin\left[\frac{2\pi}{N} i' j\right][U(i+i') - U(i-i')], \quad (14)$$

and

$$S\cdot f = \frac{\hbar}{\tau}\left\{f(i,j) - \frac{\delta k f_0(i,j)}{2\pi\rho_0(i)}\sum_{j'=1}^{N} f(i,j')\right\}. \quad (15)$$

Thus the discrete time-independent Wigner function equation is expressed as

$$[T+V+S]\cdot f = BC \quad (16)$$

BC is the value of Wigner function at the boundaries. The time-dependent Wigner function equation can be

written as

$$\frac{\partial f}{\partial t} = \frac{\Xi}{i\hbar} f, \tag{17}$$

where operator Ξ is given by

$$\Xi = i\left(T + V + S\right). \tag{18}$$

T, V, and S are the drift, potential, and scattering terms, respectively. The solution of this equation is

$$f\left(t + \delta t\right) = \exp\left(-\frac{i\Xi}{\hbar} t\right) f\left(t\right) = \frac{1 - \dfrac{i\Xi}{2\hbar} t}{1 + \dfrac{i\Xi}{2\hbar} t}. \tag{19}$$

The equation may be written as

$$\left[-2\hbar/\delta t + \Xi\right]\left[f\left(t + \delta t\right) + f\left(t\right)\right] = -4\hbar f\left(t\right)/\delta t. \tag{20}$$

In the discretized equation, the drift term gives the boundary condition, which does not change with time. Thus, we have

$$\left[-2\hbar/\delta t + \tilde{\Xi}\right]\left[f\left(t + \delta t\right) + f\left(t\right)\right] = -4\hbar f\left(t\right)/\delta t + 2BC, \tag{21}$$

where $\tilde{\Xi}$ is the operator defined by equation (19) without considering the boundary conditions of the Wigner function BC. In the whole calculation, we neglect the difference of the dielectric functions in different region of the device and the effective mass of electrons in the device.

Poisson equation (PE) is a highly nonlinear equation and the discretization of the PE is trivial. It is not suitable to directly solve this equation in the iterative coupled Wigner-Poisson equations. We consider the change of the potential $\psi = \psi_0 + \delta\psi$. Substituting the change of potential into equation (7), we obtain

$$\frac{d^2 \delta U\left(x\right)}{dx^2} = -\frac{d^2 \delta U_0\left(x\right)}{dx^2} + \frac{q^2}{\varepsilon}\left(N_d - n\left(x\right)\right). \tag{22}$$

Discretizing the above equation in the device space domain, we have

$$\begin{aligned} &-\frac{1}{2}\delta U\left(i-1\right) + \delta U\left(i\right) - \frac{1}{2}\delta U\left(i+1\right) = \\ &-\frac{1}{2}\delta U\left(i-1\right) - U\left(i\right) + \frac{1}{2}\delta U\left(i+1\right) - \frac{q^2 \Delta x^2}{2\varepsilon}\left(N_d - n_0\left(x\right)\right). \end{aligned} \tag{23}$$

Incorporating the boundary condition

$$\begin{cases} \delta U\left(0\right) = 0 & \delta U\left(N_x + 1\right) = 0 \\ U\left(0\right) = V_0 & U\left(N_x + 1\right) = V_b \end{cases} \tag{24}$$

the matrix form of the Poisson equation is written as

$$M \cdot \delta U = P, \tag{25}$$

where

$$M = \begin{bmatrix} 1 & -1/2 & 0 & \cdots & \cdots & 0 \\ -1/2 & 1 & -1/2 & 0 & \cdots & 0 \\ & & \vdots & & & \\ & & \vdots & & & \\ 0 & \cdots & 0 & -1/2 & 1 & -1/2 \\ 0 & \cdots & \cdots & 0 & -1/2 & 1 \end{bmatrix}, \tag{26}$$

and

$$\delta U = \begin{bmatrix} \delta U(1) \\ \vdots \\ \delta U(N_x) \end{bmatrix} \quad P = \begin{bmatrix} P(1) \\ \vdots \\ P(N_x) \end{bmatrix} \tag{27}$$

with

$$\begin{aligned} p\left(1\right) = &-U\left(1\right) + \frac{1}{2}U\left(2\right) \\ &-\frac{1}{2}\left[\frac{q^2 \Delta x^2}{\varepsilon}\left(N_d - n_0\left(1\right)\right) - V_0\right] \end{aligned} \tag{28}$$

$$\begin{aligned} p\left(N_x\right) = &-\frac{1}{2}U\left(N_x - 1\right) - U\left(N_x\right) \\ &-\frac{1}{2}\left[\frac{q^2 \Delta x^2}{\varepsilon}\left(N_d - n_0\left(N_x\right)\right) - V_b\right]. \end{aligned} \tag{29}$$

In our simulation, we first approximate the conduction-band profile by a square well potential and get $n(x)$ from equation (1) and equation (8). The density of electrons is substituted into the Poisson equation and then the new conduction-band profile

$$U\left(x\right) = u\left(x\right) + \Delta_c\left(x\right) \tag{30}$$

is obtained, where $\Delta_c\left(x\right)$is the offset of the band edge. Using this new conduction-band profile at the next time step, the Wigner function equation is solved again. This iteration continues until a steady-state or a preassigned time value is achieved by a simultaneous solution of both equations (1) and (7).

3 Numerical results and discussion

The I-V characteristics in the single quantum well were numerically studied by Zhao et al. [10]. Here we study the quantum well with an inserted potential well layer. The parameters used in our simulation are as follows. The momentum and position spaces are broken into 134 and 160 points, respectively. The donor density is $N_d = 2.0 \times 10^{18}$ particles/cm^3. The compensation ratio for scattering calculations is 0.3, the barrier, main quantum well and inserted potential well widths are 3, 5 and 1.38 nm, respectively, the simulation box is 55 nm, the barrier potential is 317 meV. The device temperature is 77 K, the effective mass of the electron is assumed to be constant and equals 0.0667 m_0. The doping extends to 3 nm before the emitter barrier and after the collector barrier; the whole

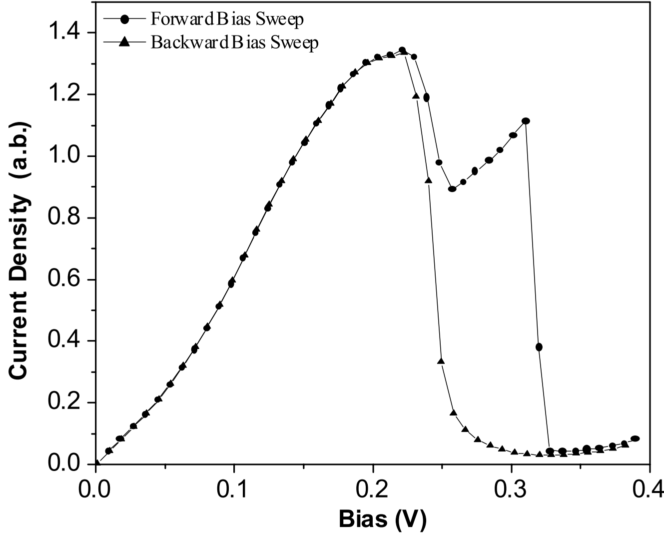

Fig. 2. I-V curves of the double-barrier structures, the data are taken from the steady states of the simulation, which is the time average value of current oscillation.

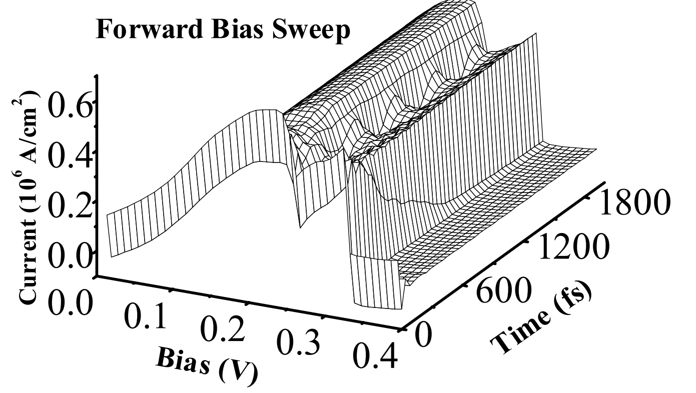

Fig. 3. The current characteristics of double-barrier structures with time and bias voltages as parameters for the case of forward bias sweep.

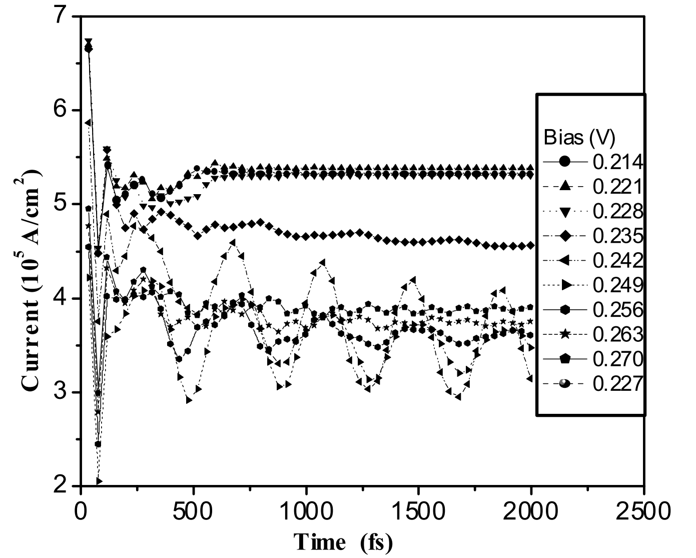

Fig. 4. The current-time characteristics of double-barrier structures in different bias voltages for the case of forward bias sweep.

quantum well region is undoped, and the method of evaluating the relaxation time can be found in reference [35].

In order to study the effect of the inserted potential well on the main quantum well structure, we first give the results of the single quantum well without the inserted layer and calculate the I-V characteristic of the resonant tunneling when the time-depended simulation reaches steady state in forward and backward bias sweep. Here, the mesh points of momentum and position spaces are 72 and 86, respectively. The current values are obtained by averaging over 2 ps time intervals. Our results are shown in Figure 2. In this figure, we find the obvious plateaulike structure and a current hysteresis phenomenon. Because of the space-charge buildup in the main quantum well, the conductance band bottom of QW will be increased, which makes the lowest-energy level in the QW be driven up, and the corresponding position of the peak of current will be shifted to the high bias.

Figure 3 shows the time-dependent current density with bias voltage in forward bias sweep. The results show that the current changes with the time, and an obvious current oscillation appears in the region of plateau-like structure, which is due to the coupling of the main well and the spacer well before the emitter barrier. In order to show clearly these current oscillations, Figure 4 gives the current-time curves in different special bias voltages. Figure 5 gives the electron density distribution of the whole device in different bias, we can find the obvious electron density distribution region in the spacer of emitter when the bias lie in the plateaulike region, and these electron density oscillations can lead to large fluctuation of electron potential, this kind potential fluctuation can form the quantum well structure in the emitter. Our calculations show that this special electron density distribution changes with the time, which leads to a high-frequency current oscillation and further affects the final current value in steady situation. Of course, there is relaxation time to form electron density distribution oscillation. A coupling of the emitter quantum well and main quantum well is formed and this coupling will further damp the decrease of the current with the increase of the bias to form a current plateau structure. The plateau structure is results from time average of the current oscillation. If we do not consider the self-consistent and time effect, there will be no plateau structure in the case of forward bias sweep, as shown in Figure 6. Figures 7 and 8 show the current density and electron density distribution of the device in the case of backward bias sweep, i.e., the bias changing from high bias to low bias. In such situation, we cannot find the obvious regular current oscillations and electron density variation region. The main reason is that, in the backward bias, there is no electron pre-accumulation in the emitter. Now we investigate the effect of the inserted potential well on the I-V curves, which can help us to

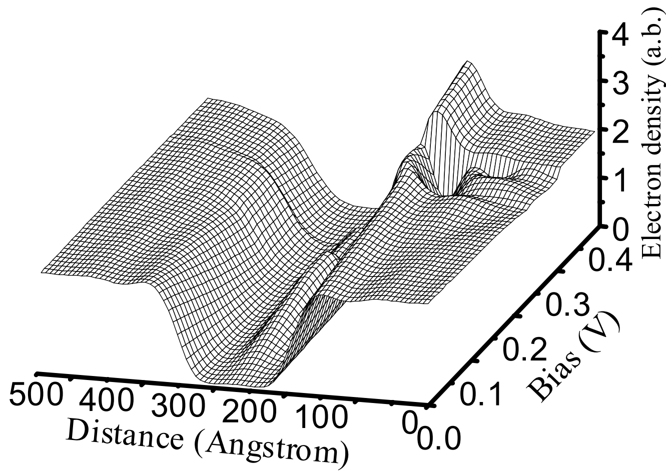

Fig. 5. The local electron density distribution of double-barrier structures with bias voltages as parameters, for the case of forward bias sweep.

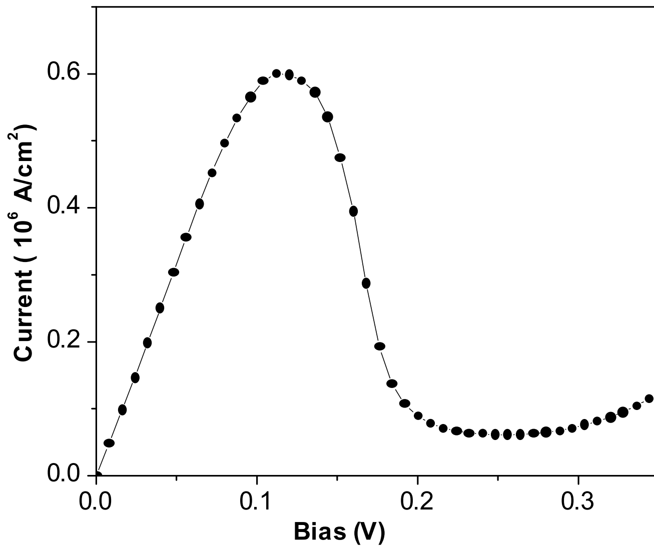

Fig. 6. I-V curves of the double-barrier structures in the forward bias voltages. The data are taken from the time-independent simulation.

understand the physical mechanism of electron transport in low-dimensional device. Our studies show that the middle thin potential well layer can affect remarkably the plateau structure and current oscillation.

In order to understand the effect from the inserted layer, we calculated the I-V curve of the steady state of the quantum well with the inserted potential well layer. The calculated results of the final current are shown in Figure 9. From the figure, it can be seen that comparing with the single quantum well without the inserted layer, there is no plateau structure, resonant bias is shifted to the low bias voltage value, and the amplitude of peak current is reduced about 8%. On the other hand, apart form the main current peak, there is no new current peak in the I-V curves, so this inserted layer does not lead to a new bound state. But the I-V curve still shows current

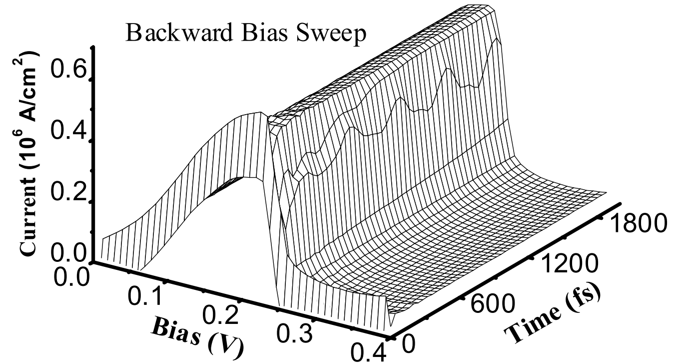

Fig. 7. The current characteristics of double-barrier structures with time and bias voltages as parameters for the case of backward bias sweep.

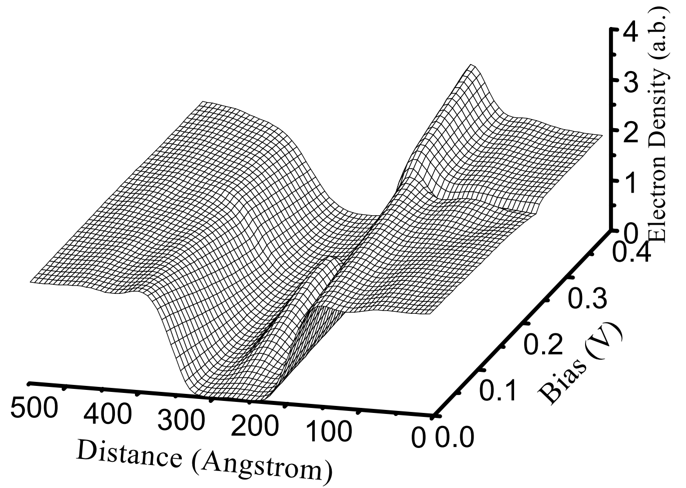

Fig. 8. The local electron density distribution of double-barrier structures with bias voltages as parameters for case of backward bias sweep.

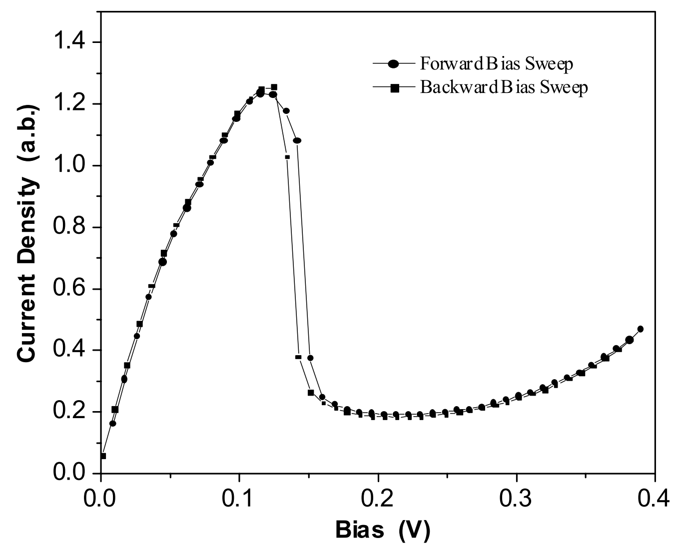

Fig. 9. I-V curves of the double-barrier structures with the inserted potential well, the data are taken from the steady states of the simulation, which is the time average value of current oscillations.

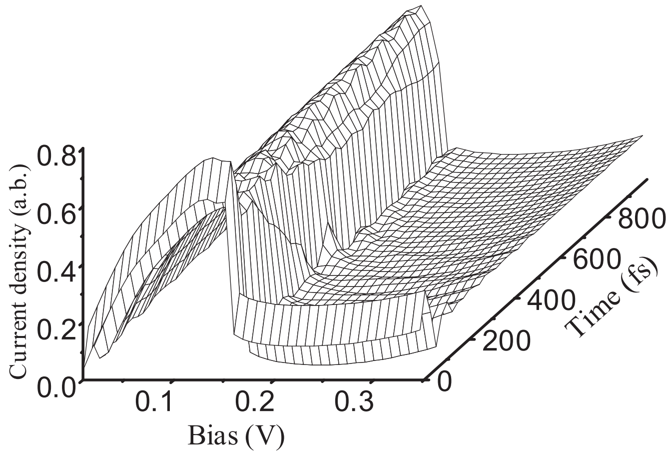

Fig. 10. The current characteristics of device with time and bias voltages as parameters, for the case of forward bias sweep. The device is a double-barrier structure with the thin inserted potential well layer.

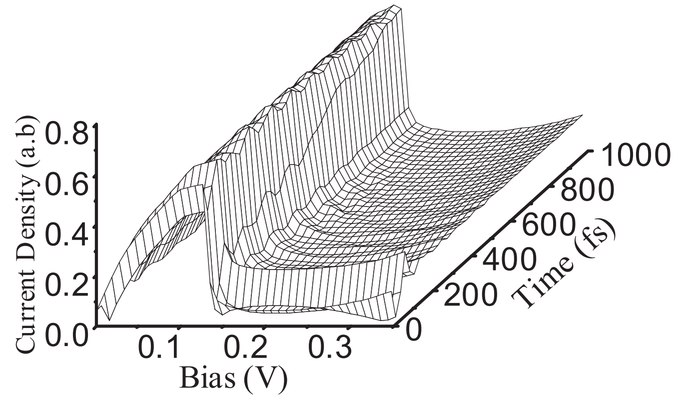

Fig. 12. The current characteristics of device with time and bias voltages as parameters, for the case of backward bias sweep. The device is a double-barrier structure with the thin inserted potential well layer.

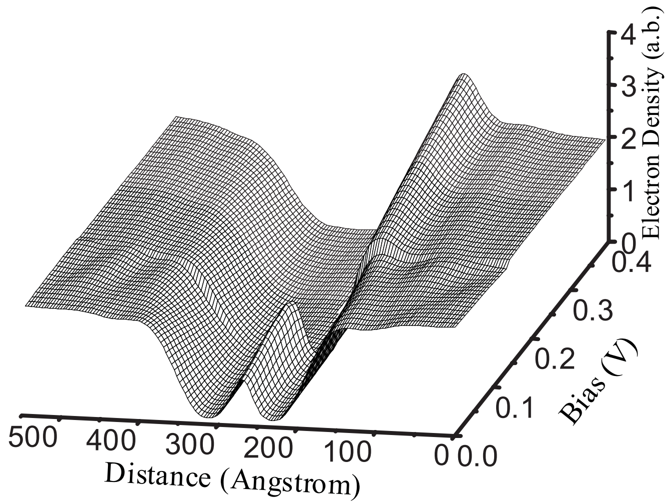

Fig. 11. The local electron density distribution with bias voltages as parameters for the case of forward bias sweep. The device is a double-barrier structure with the thin inserted potential well layer.

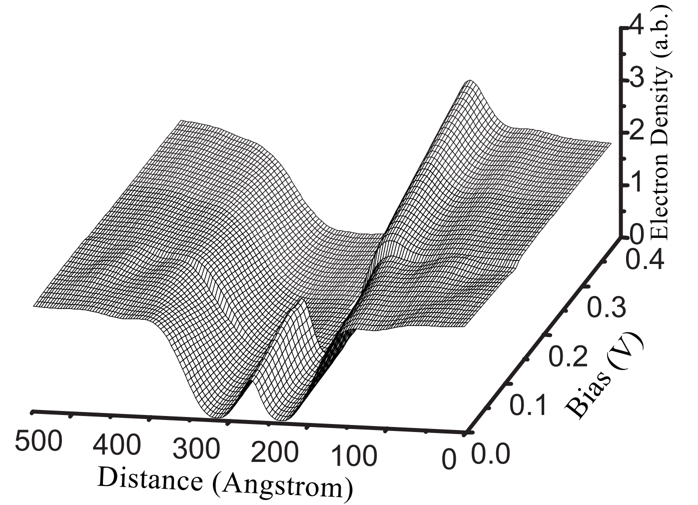

Fig. 13. The local electron density distribution with bias voltages as parameters for the case of backward bias sweep. The device is a double-barrier structure with the thin inserted potential well layer.

hysteresis phenomenon, the width of current hysteresis curve is reduced in the device with the inserted potential well layer. This shows that the inserted layer not only affect the electron behaviour in the main well, but also affect the electron density oscillation in the emitter. This is validated by the calculations of the current and local electron density distribution. In Figures 10 and 11, we show the situation in the forward bias sweep. In Figure 10, the results show that under certain bias there are still some current oscillations with time. But comparing with the results of Figure 3, the obvious reduction of the amplitude of the current oscillation has been found, and this current oscillation lacks the regulation. Comparing to Figure 5, in Figure 11, we do not find the electron density distribution oscillation in the emitter region, and when the bias voltage passes the resonance bias, the electron buildup in the main well disappears. All these phenomena show that the inserted potential well can affect the electron density variation in main well and the emitter region. This is because that the potential well layer adjusts the energy level of main QW and reduces the electron buildup in the main QW. This effect leads to a rapid collapse of emitter QW in the emitter and the current plateau disappears for the forward bias sweep. So the electron buildup and the change of electron density distribution in the emitter together affect the final I-V curves. From the Figures 12 and 13, it can be seen that in the backward bias sweep, the situation is similar to that in the forward bias sweep. But, comparing with single quantum well shown in Figure 7, the current curves show some oscillations in certain bias voltage of the backward bias sweep. On the other side, from Figures 11 and 13, the inserted layer does not affect remarkably the electron accumulation in the main well for the forward and backward bias sweep.

4 Conclusion

For the quantum well device with the thin inserted potential well layer, by using a time-dependent finite-difference technique, we numerically solved the coupled Wigner-Poisson equations. Comparing to the normal single quantum well device, the inserted potential well layer affects strongly the electron density distribution and current curves, which damps the formation of the potential well in the emitter region and further affects the current oscillations. Therefore, the inserted potential well layer leads to the plateau disappearing and current hysteresis curve narrower. Using this inserted layer technique we can adjust the resonant tunneling structure (RTS) device to show the different degree of current hysteresis. We conclude that any attractive potential will affect the width of the hysteresis of current and the current oscillation, which can damp the formation of the current plateau. These results can extend qualitatively to the case of the quantum well with the quantum dot layer. All these show that in the fabrication of the high-frequency device, we must reduce the presence of the attractive potential impurities and defection.

We thank the Prof. H.L. Cui and Dr. Peiji Zhao of Steven Institute of Technology, USA, for the help in the method of calculations. The work was supported by the State Key Development Program for Basic Research of China (Grant No. G2000067107) and the National Foundation of Natural Science in China (Grants No 10404022)

References

1. Bo Su, V.J. Goldman, M. Santos, M. Shayegan, Appl. Phys. Lett. **58**(7), 747 (1991)
2. A.D. Martin, M.L.F. Lerch, P.E. Simmonds, L. Eaves, Appl. Phys. Lett. **64**(10), 1248 (1994)
3. R.K. Kawakami, E. Rotenberg, Hyuk J. Choi, E.J. Escorcia-Aparicio, M.O. Bowen, J.H. Wholfe, E. Arenholz, Z.D. Zhang, N.V. Smith, Z.Q. Qiu, Nature **398**, 132 (1999)
4. D. Grundler, Phys. Rev. Lett. **84**, 6074 (2000)
5. D. Snoke, S. Denev, Y. Liu, L. Pfeiffer, K. West, Nature **418**, 754 (2002)
6. S.Q. Murphy, J.P. Eisenstein, L.N. Pfeiffer, K.W. West, Phys. Rev. B **52**(20), 14825 (1995)
7. N. Tansu, Jeng-Ya Yeh, Luke J. Mawst, Appl. Phys. Lett. **83**(11), 2112 (2003)
8. T. Ohtsuka, L. Schrottke, R. Hey, H. Kostial, H.T. Grahn, J. Appl. Phys. **94**(4), 2192 (2003)
9. K.L. Jensen, F.A. Buot, Phys. Rev. Lett. **66**, 1079 (1991)
10. Peiji Zhao, H.L. Cui, D.L. Woolard, Phys. Rev. B **63**, 075302 (2001)
11. Y.B. Yu, T.C. Au Yeung, W.Z. Shangguan, K.C. Hin, Phys. Rev. B **63**, 205314 (2001)
12. W.Z. Shangguan, T.C. Au Yeung, Y.B. Yu, C.H. Kam, Phys. Rev. B **65**, 235315 (2002)
13. V.J. Goldman, D.C. Tsui, J.E. Cunningham, Phys. Rev. Lett. **58**, 1256 (1987)
14. L.L. Chang, L. Esaki, R. Tsu, Appl. Phys. Lett. **24**, 593 (1974)
15. T.C.L.G. Sollner, Phys. Rev. Lett. **59**, 1622 (1987)
16. T.J. Foster, M.L. Leadbeater, L. Eaves et al., Phys. Rev. B **39**, 6205 (1989)
17. A. Zaslavsky, V.J. Goldman, D.C. Tsui, J.E. Cunningham, Appl. Phys. Lett. **53**, 1408 (1988)
18. E.S. Alves, L. Eaves, M. Henini et al., Electronics Lett. **24**, 1190 (1988)
19. M.L. Leadbeater, E.S. Alves, F.W. Sheard et al. J. Phys.: Condens. Matter **1**, 10605 (1989)
20. F.W. Sheard, G.A. Toombs, Appl. Phys. Lett. **52**, 1228 (1988)
21. P.C. Main, T.J. Foster, P. Medonnell, L. Eaves, M.J. Gompertz, N. Mori, J.W. Sakai, M. Henini, Phys. Rev. B **62**(24), 16721 (2000)
22. M. Roberts, Y.C. Chung, S. Lyapin, N.J. Mason, R.J. Nicholas, P.C. Klipstein, Phys. Rev. B **65**, 235326 (2002)
23. L. Hirsch, A.S. Barriere, J. Appl. Phys. **94**(8), 5014 (2003)
24. Gyungock Kim, Dong Wan Roh, Seung Won Paek, Appl. Phys. Lett. **83**(4), 695 (2003)
25. Hiroya Ikeda, Masanori Iwasaki, Yasuhiko Ishihawa, Michiharu Tabe, Appl. Phys. Lett. **83**(7), 1456 (2003)
26. A. Rosenauer, D. Gerthsen, D. Van Dyck, M. Arzberger, G. Böhm, G. Abstreiter, Phys. Rev. B **64**, 245334 (2001)
27. F. Pulizzi, E.E. Vdovin, K. Takehana, Yu.V. Dubrovskii, A. Patane, L. Eaves, M. Henini, P.N. Brunkov, G. Hill, Phys. Rev. B **68**, 155315 (2003)
28. G.B. Galiev, V.E. Kaminskii, V.G. Mokerov, V.A. Kulbachinskii, R.A. Lunin, I.S. Vasilevskii, A.V. Derkach, Semiconductors **37**(6), 686 (2003)
29. Z. Barticevic, P. Vargas, M. Pacheco, D. Altbir, Phys. Rev. B **68**, 155306 (2003)
30. G.H. Kim, J.T. Nicholls, S.I. Khondaker, I. Farrer, D.A. Ritchie, Phys. Rev. B **61**(16), 10910 (2000)
31. E.E. Vdovin, Yu.N. Khanin, Yu.V. Dubrovskii, P.C. Main, L. Eaves, M. Henini, G. Hill, Phys. Rev. B **67**, 205305 (2003)
32. A. Patane, A. Polimeni, L. Eaves, P.C. Main, M. Henini, A.E. Belyaev, Yu.V. Dubrovskii, P.N. Brounkov, E.E. Vdovin, Yu.N. Khanin, Phys. Rev. B **62**(20), 13595 (2000)
33. B.R.A. Neves, J.F. Sampaio, E.S. Alves et al., Superlattices, Microstructures **20**, 181 (1996)
34. D.K. Ferry, H.L. Grubin, Solid State Phys. **49**, 283 (1995).
35. F.A. Buot, K.L. Jensen, Phys. Rev. B **42**, 9429 (1990)
36. W.R. Frensley, Rev. Mod. Phys. **62**(3), 745 (1990)